iScience

CellPress
OPEN ACCESS

Article

AXL cooperates with EGFR to mediate neutrophil elastase-induced migration of prostate cancer cells

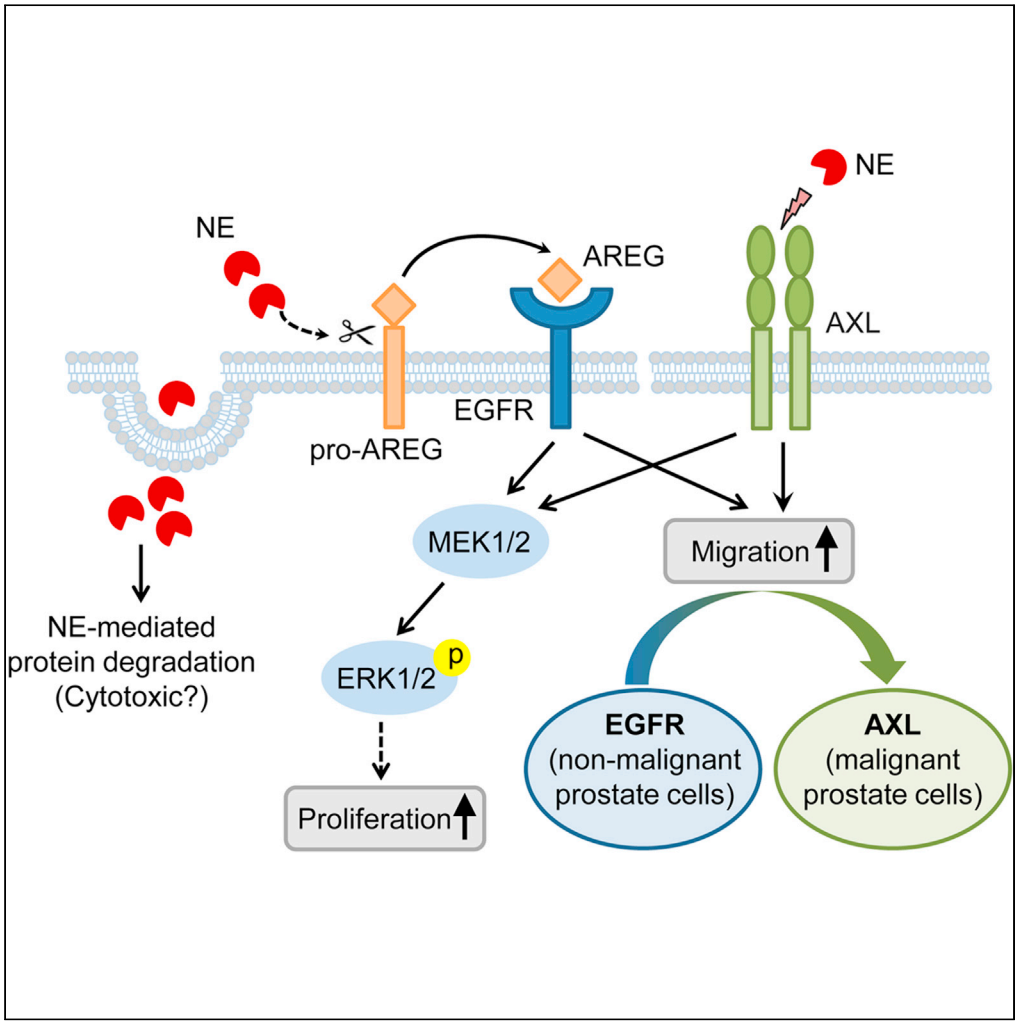

Zhiguang Xiao, Stephen R. Hammes

zhiguang_xiao@urmc.rochester.edu

Highlights

NE triggers the release of AREG to activate EGFR/ERK signaling in prostate cells

AREG-EGFR axis is critical in NE-induced migration of nonmalignant prostate cells

NE promotes prostate cancer cell migration via AXL rather than EGFR

Accessibility of NE in prostate cells may be associated with cell malignancy

Xiao & Hammes, iScience *24*, 103270
November 19, 2021
https://doi.org/10.1016/j.isci.2021.103270

iScience

CellPress
OPEN ACCESS

Article

AXL cooperates with EGFR to mediate neutrophil elastase-induced migration of prostate cancer cells

Zhiguang Xiao[1,2,*] and Stephen R. Hammes[1]

SUMMARY

Neutrophil elastase (NE) promotes multiple stages of tumorigenesis. However, little is known regarding the molecular mechanisms underlying its stimulatory role. This study shows that NE triggers dose-dependent ERK signaling and cell migration in a panel of prostate cell lines representing the spectrum of prostate cell malignancy. All cell lines tested internalize NE; however, NE endocytosis is not required for ERK activation. Instead, NE acts extracellularly by stimulating the release of amphiregulin to initiate EGFR-dependent signaling. Inhibiting amphiregulin's biological activity with neutralizing antibodies, as well as gene silencing of amphiregulin or EGFR, attenuates NE-induced migration in normal and benign prostatic cells. Alternatively, in prostate cancer cells, knockdown of receptor tyrosine kinase AXL, but not EGFR, impairs both basal and NE-stimulated migration. When prostate cells progress to malignancy, the switch from EGFR-to AXL-dependence in NE-mediated migration implies the potential combined application of EGFR and AXL targeted therapy in prostate cancer treatment.

INTRODUCTION

Prostate cancer is the second leading cause of cancer-related death in men (Siegel et al., 2020). Treatment options for advanced prostate cancer such as radiation, androgen deprivation, and chemotherapy are often initially efficient at shrinking tumor size and slowing tumor progression; however, over time these therapies lose effectiveness. In addition to intrinsic heterogeneities of tumor cells, growing evidence suggests that their interactions with the surrounding microenvironment, specifically infiltrating immune cells, contribute significantly to cancer progression and therapeutic resistance. Through direct contact or secreting inflammatory stimuli, these diverse immune cells engage in extensive and dynamic crosstalk to promote tumor growth. We recently showed that granulocytic myeloid cells accumulated in the peripheral blood and local tumors in human prostate cancer cell xenografts as well as in prostate-specific *Pten*-null mouse models (Lerman et al., 2017, 2019). Immunodepletion of these myeloid cells markedly reduced tumor growth. Furthermore, inhibition of myeloid cell-derived neutrophil elastase (NE) similarly mitigated prostate tumor growth in both models. These results suggest that innate immunity via granulocyte-derived NE may play an important role in prostate cancer progression.

NE is a serine protease stored in neutrophil azurophilic granules that is traditionally known for its function in degrading invading pathogens engulfed in the phagolysosome (Korkmaz et al., 2010). During chronic disease or infection, NE is released at high concentrations to the sites of inflammation as a result of neutrophil activation. In addition to tissue remodeling, extracellular NE functions as a regulator of the immune response by actively processing chemokines, cytokines, and specific cellular receptors (Meyer-Hoffert, 2009). Accordingly, inhibition of NE limits neutrophil infiltration and NE-mediated tissue damage in various inflammatory disorders, including ischemia, lung injury, and arthritis (Pham, 2006). NE is also implicated as pro-tumorigenic, with evidence showing reduced tumor growth in mice with genetic deletion or pharmacological inhibition of NE (Starcher et al., 1996; Houghton et al., 2010; Lerman et al., 2017; Caruso et al., 2015). In fact, elevated serological NE positively correlates with advanced stages and poor survival in lung cancers (Yamashita et al., 1997). Similarly, NE appears up-regulated in cases of breast cancer, glioma, and colon adenocarcinoma (Foekens et al., 2003; Iwatsuki et al., 2000; Ho et al., 2014).

[1]Department of Medicine, University of Rochester Medical Center, Rochester, NY 14620, USA

[2]Lead contact

*Correspondence: zhiguang_xiao@urmc.rochester.edu

https://doi.org/10.1016/j.isci.2021.103270

Several mechanisms have been proposed for NE-mediated cellular responses that potentiate cancer development. With regard to prostate cancer, NE may contribute to tumor growth by directly increasing proliferation, migration, and invasion of cancer cells (Lerman et al., 2017). However, how NE signals to enhance these processes remains unclear. As a protease, NE has broad substrate specificity. Evidence suggests that NE may function intracellularly, with studies demonstrating that lung adenocarcinoma cells can engulf NE, leading to NE-mediated degradation of insulin receptor substrate-1 (IRS-1) and subsequent enhancement of PI3K-AKT signaling (Houghton et al., 2010; Gregory et al., 2012). Mechanistically, NE endocytosis was shown to be mediated by clathrin pits or neuropilin-1, independent of its enzymatic activity (Gregory et al., 2012; Kerros et al., 2017). Alternatively, NE may trigger tumor cell processes from the cell membrane specifically by activating the epidermal growth factor receptor (EGFR) signaling. For instance, NE in lung cells, via EGFR transactivation, activates P38/NF-kB cascade mediated IL-8 transcription (Kuwahara et al., 2006). NE may also cause the release of EGFR ligands such as EGF and TGFα, leading to EGFR-dependent ERK activation and MUC5AC induction (Shao and Nadel, 2005; DiCamillo et al., 2002, 2006). Similarly, NE was shown to promote cell proliferation and migration in esophageal cancer cells via shedding of TGFα, PDGF, and VEGF, with possible activation of their corresponding receptor tyrosine kinases (RTKs) (Wada et al., 2006). The importance of EGFR signaling has been implicated in normal prostate growth and neoplastic development (Kambhampati et al., 2005). Histological examination of EGFR expression in prostatic cancer tissues revealed that EGFR was overexpressed in 18-30% of adenocarcinoma and significantly associated with high Gleason score, high serum prostate-specific antigen (PSA), and worse outcomes (Di Lorenzo et al., 2002; Schlomm et al., 2007; De Muga et al., 2010; Hashmi et al., 2019), implicating its role as a prognostic biomarker in prostate cancer.

Given the aforementioned pleiotropic roles of NE, here we explored the effects of NE on EGFR-mediated signaling and migration in human prostate cells by introducing a panel of cell lines derived from normal, benign, and malignant prostate tissues. Our results reveal a stimulatory activity of NE on EGFR tyrosine phosphorylation, downstream mitogenic signaling, and migration in all cell lines. We also delineated the molecular mechanism involved in these regulations, demonstrating that NE triggers ERK1/2 activation in both normal and neoplastic prostate cells by releasing a soluble form of amphiregulin (AREG) to initiate EGFR-dependent signaling. Gene silencing of EGFR or AREG prevents NE-induced migration of non-malignant prostate cells; however, in prostate cancer cells, the activation of AXL acts as an alternative receptor tyrosine kinase in response to NE and may mediate resistance to EGFR targeted therapy.

RESULTS

Endocytosis of neutrophil elastase (NE) in prostate cancer cells is dynamin-dependent

NE-mediated ERK phosphorylation has been demonstrated in various cell types, including prostate cancer (Lerman et al., 2017). Here, we began by examining/confirming NE-induced ERK activation in a panel of human prostate cell lines representing the spectrum of prostate cell malignancy: NHPrE1 (normal), BPH-1 (benign), and DU145 (cancerous) (Table S1). As expected, the addition of NE led to a dose-dependent activation of ERK1/2 in all cell lines (Figure 1A). Similar ERK activation was further observed in BHPrE1 (normal), RWPE1 (HPV18 transformed primary epithelial cells therefore considered benign), and PC3 (cancer) prostate cells (Figure S1, top two panels). Of note, NE concentrations used on our cell lines are within the range of its expected physiological concentrations (~50 nM = 1.5 μg/mL).

Previous studies showed that clathrin pit-mediated entry of NE into tumor cell endosomes, including lung and breast, is required for its cell proliferative effects (Houghton et al., 2010; Mittendorf et al., 2012). Therefore, we examined whether prostate cancer cells, as well as non-malignant prostate cells, could also internalize NE. By culturing cells in NE–supplemented medium, immunofluorescence staining revealed intracellular trafficking of NE with predominant perinuclear localization, yet the accessibility varied among cell lines and was closely associated with cell malignancy (Figure 1B). Specifically, only a few cells in NHPrE1 normal prostatic colonies were able to engulf NE, whereas poorly differentiated DU145 cancer cells exhibited the most immunoreactivity, with close to 100% positivity for NE cytoplasmic staining (Figure 1B). Western blot analysis further showed that prostate cells did not produce NE and that NE entry occurred in a dose-dependent fashion in all three cell lines, as well as in BHPrE1, RWPE1, and PC3 prostate cells (Figures 1C and S1, bottom panel). We next applied Dynasore treatment, a dynamin inhibitor that prevents clathrin-mediated internalization, on DU145 prostate cancer cells since they had the most efficient NE uptake. Indeed, Dynasore strongly reduced detectable levels of NE in DU145 cells (Figure 1D, top), confirming that dynamin is

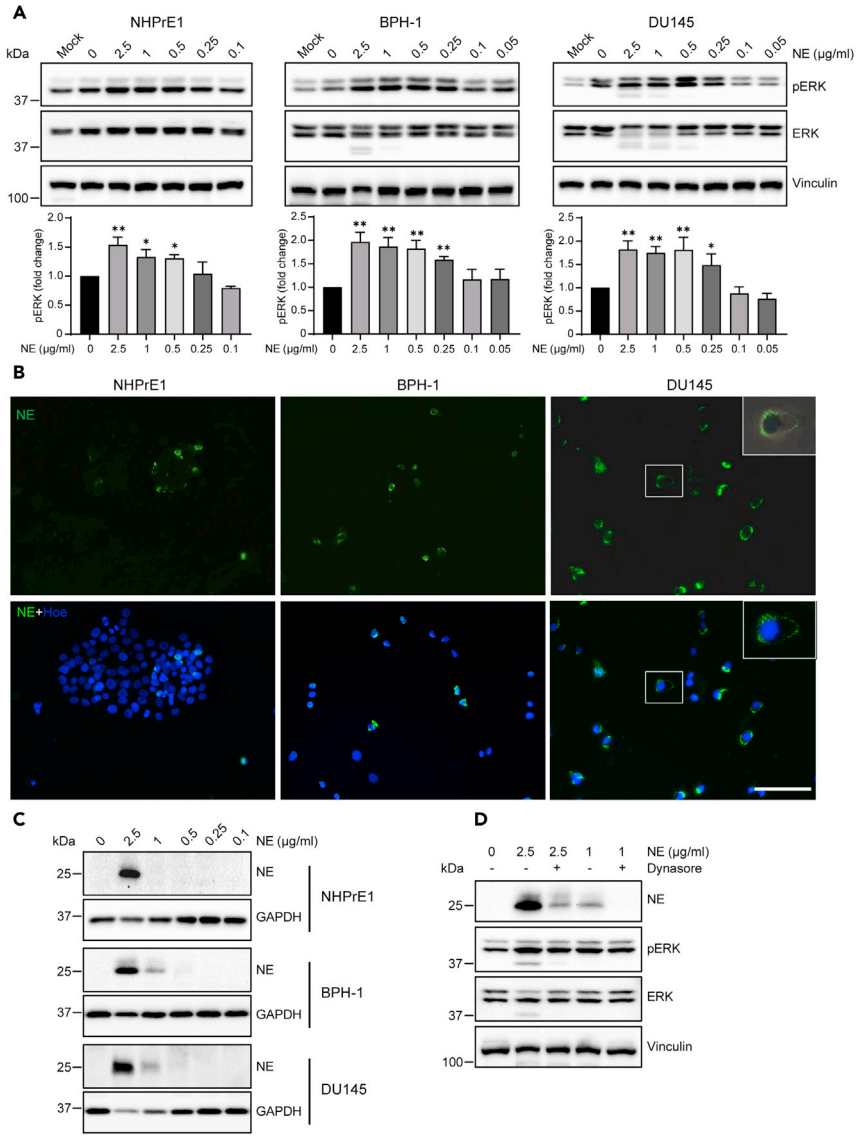

Figure 1. ERK activation is not mediated by NE endocytosis

(A) Cells were serum-starved overnight and then stimulated with NE (doses as indicated) or vehicle (0 μg/mL of NE) for 10 min. Cell lysates were immunoblotted with anti-phospho ERK antibody followed by re-probing the same membranes with anti-total ERK and Vinculin antibodies. Density quantifications of phosphorylated relative to total ERK are shown on the histograms. Data are mean ± SEM from n = 3 experiments. The asterisks indicate differences between NE versus vehicle treatment. *$p < 0.05$ and **$p < 0.01$ by one-way ANOVA Dunnett test. Mock: cells cultured in complete medium and no treatment.

(B) Immunofluorescence analysis of cells with NE (green) and the nuclear stain Hoechst 33342 (blue). Cells, after overnight starvation, were stimulated for 10 min with NE at 2.5 μg/mL (n = 2). The enlarged image in the upper right is NE staining merged with phase contrast. Scale bar: 100 μm.

(C and D) Serum-starved cells were incubated with NE (doses as indicated), or vehicle for 10 min with (D) or without (C) 30 min of Dynasore (80 μM) pretreatment. Cells lysates prepared for Western blot analysis of NE, phospho and total ERK (n = 2).

See also Figure S1 and Table S1.

required for NE endocytosis of prostate cells. However, little or no changes in NE-triggered ERK phosphorylation were associated with this treatment (Figure 1D), indicating that NE endocytosis is not necessary for ERK activation in prostate cells.

NE-mediated ERK activation is EGFR dependent

Eliminating the possibility of ERK activation through intracellular NE, we then shifted to the extracellular function of NE, focusing on its proteolytic involvement in the activation of EGFR dependent signaling. By examining a panel of human prostate cell lines, we found EGFR was strongly expressed in cell lines derived from the normal and benign prostatic gland, and there was a preferential expression in androgen-independent (C4-2, PC3, and DU145) versus androgen-dependent (LNCap, LAPC-4, VCap, and 22RV1) cells (Figure 2A).

With confirmed EGFR expression in our selected cell lines, we next assessed whether NE-induced ERK activation was mediated by EGFR phosphorylation. Dose-response studies in serum-starved non-malignant NHPrE1 and BPH-1 cells revealed a modest increase of NE-induced EGFR phosphorylation, whereas, in DU145 cancer cells, EGFR was constitutively phosphorylated despite serum deprivation, with little or no increase upon NE stimulation due to the high basal phosphorylation level (Figure S2). Treatment of cells with AG1478, a selective EGFR tyrosine kinase inhibitor, almost completely prevented NE-promoted ERK phosphorylation in all three cell lines, indicating that EGFR kinase activity is required for NE-mediated ERK activation (Figure 2B).

To ascertain the EGFR dependent stimulatory effect of NE, we abrogated EGFR expression in the three cell lines using pooled small interfering RNA (siRNA) induced knockdown, noting that EGFR deletion conferred a significant inhibition in NE-mediated ERK phosphorylation (Figure 2C). Together, these data implicate that EGFR acts as a critical mediator in NE-induced ERK activation in prostate cells.

Ectodomain shedding of amphiregulin (AREG) regulates NE-induced EGFR/ERK signaling

EGFR activation requires ligand-induced dimerization, which leads to EGFR kinase domain cross-phosphorylation and subsequent initiation of downstream signaling cascades. To determine which ligand(s) are specifically involved in the activation of NE-induced EGFR dependent signaling in prostate cells, we first measured intracellular mRNA expression levels of seven EGFR agonists (EGF, HBEGF, TGFA, AREG, BTC, EPGN, and EREG). Quantitative RT-PCR identified AREG as the dominant transcript in all cell types tested (Figures 3A and S3). In addition, the *AREG* mRNA abundance was strikingly higher in non-malignant NHPrE1, BHPrE1, RWPE1, and BPH-1 cells compared to DU145 and PC3 cancer cells (Figures 3A and S3). Western blot analysis further revealed high AREG protein expression in normal and benign prostatic cells, and lower expression in all cancer cell lines (Figure 3B).

AREG is synthesized as a 252-amino acid transmembrane precursor (pro-AREG), and extracellular cleavage of pro-AREG generates a mature soluble ligand that engages in autocrine or paracrine activation of EGFR (Plowman et al., 1990). To determine whether treatment of prostate cells with NE triggers the release of AREG, cells were serum-starved for 18 h before NE stimulation and supernatants collected for enzyme-linked immunosorbent assay (ELISA) evaluation. All three cell lines tested were able to release AREG in starved conditions (Figure 3C), indicating a potential role of AREG in autocrine-regulated cellular response in these cells. NE stimulation promoted AREG secretion and peaked with NE at 0.5 and 1 μg/mL, whereas detectable AREG declined with higher doses of NE, perhaps because of NE-mediated non-specific proteolysis of AREG or to direct toxic effects of NE (Figure 3C).

We next assessed whether soluble AREG is responsible for NE-mediated ERK phosphorylation by pretreatment of serum-starved cells with anti-AREG antibody (α-AREG) to neutralize AREG before NE stimulation. Previous work had shown that application of α-AREG specifically blocked AREG-induced EGFR phosphorylation and had no effect on EGF, HBEGF, or TGFA (Gusenbauer et al., 2015). Treatment with α-AREG almost completely abrogated NE-induced ERK phosphorylation in BPH-1 cells and caused a moderate but significant reduction in NHPrE1 cells (Figure 3D, left and middle panels). Inhibition was qualitatively present but not statistically significant in DU145 cells (Figure 3D, right panel). Together, these data implicate NE-stimulated proteolytic cleavage and release of AREG as an important mechanism modulating EGFR/ERK activation in prostate cells, perhaps more so in benign prostate cells versus those that are carcinogenic.

AREG-EGFR axis is essential in NE-induced migration of benign prostatic cells

The ability for cells to migrate is essential for maintaining physical functions and pathologic development. Our previous study demonstrated that NE directly promoted the migration of prostate cancer cells (Lerman

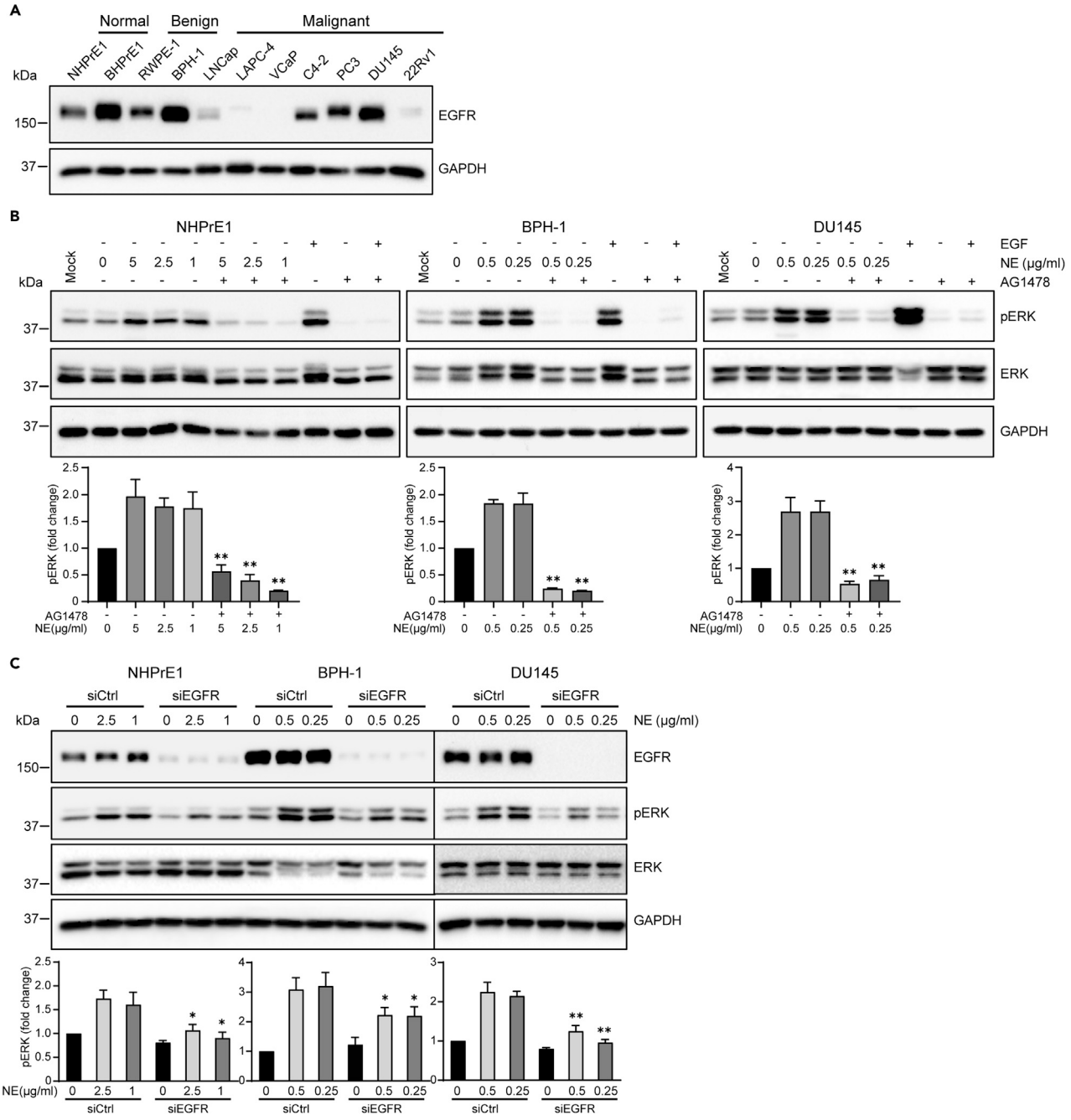

Figure 2. EGFR inhibition suppresses NE-mediated ERK activation

(A) Indicated cell lines were lysed and prepared for Western blot analysis of EGFR (n = 2).

(B) Serum-starved NHPrE1, BPH-1, and DU145 cells were pretreated with AG1478 (500 nM) or DMSO for 30 min and then stimulated with NE (doses as indicated), EGF (50 ng/mL), or vehicle for 10 min. Cells treated with EGF served as positive controls. Blots were probed with anti-phospho ERK antibodies followed by stripping and re-probing the same membranes with anti-total ERK and GAPDH antibodies. AG1478 induced pERK inhibitions quantified and displayed on histograms. The asterisks indicate the difference between NE versus AG1478 + NE. Data represent mean ± SEM from n = 3 experiments. **p < 0.01 by one-way ANOVA Sidak test. Mock: cells cultured in complete medium and no treatment.

(C) Cells transfected for approximately 55 h with EGFR specific siRNA (siEGFR) or scramble control (siCtrl), and then serum-starved overnight prior to 10 min stimulation with NE (doses as indicated) or vehicle. Immunoblots for EGFR, pERK, ERK, and GAPDH are shown. siEGFR mediated pERK inhibitions quantified and displayed on histograms. The asterisk indicates the difference between siCtrl + NE versus siEGFR + NE. Data represent mean ± SEM from n = 3 experiments. p values determined by two-way ANOVA Sidak test. *p < 0.05, **p < 0.01.

See also Figure S2.

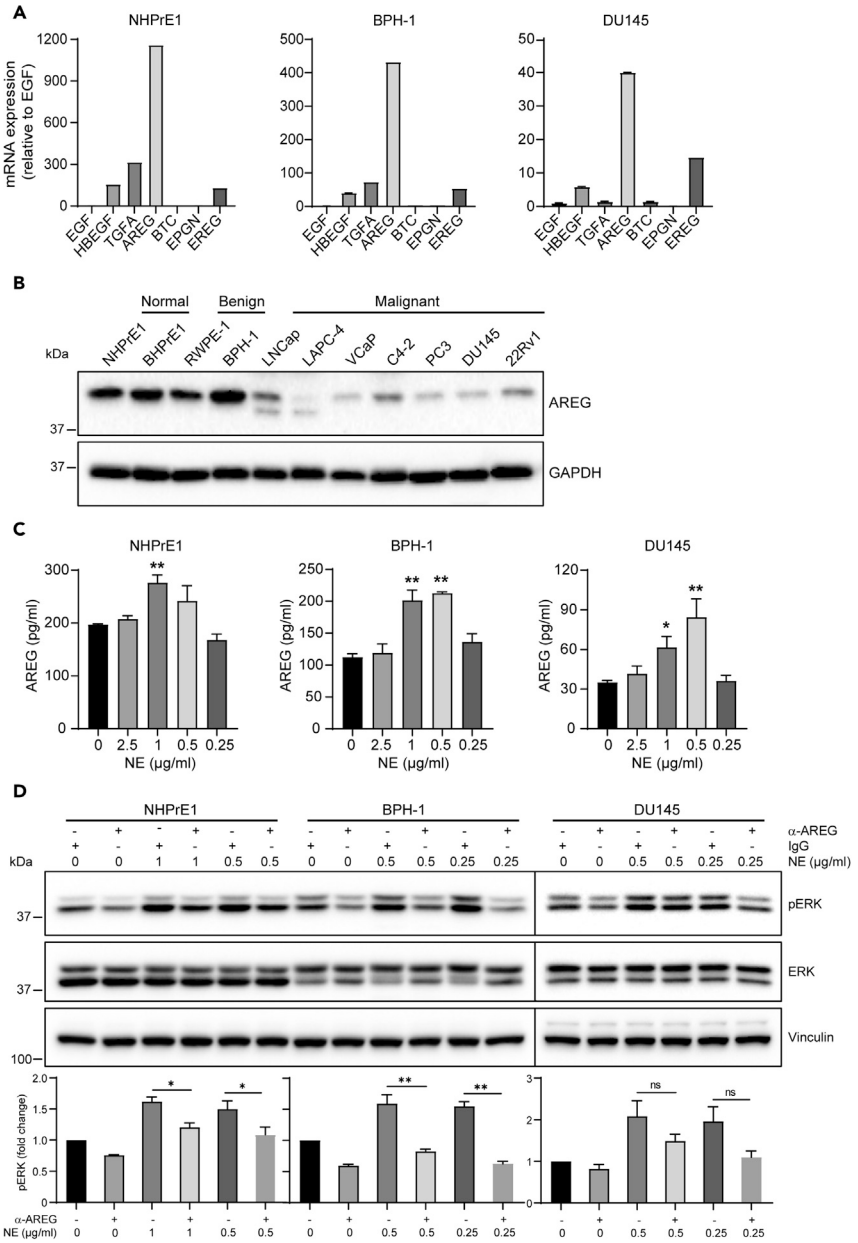

Figure 3. NE-initiated EGFR/ERK signaling is mediated by the release of amphiregulin (AREG) in NHPrE1 and BPH-1 cells

(A) The differential expressions of EGFR ligands in NHPrE1, BPH-1, and DU145 cells were assessed by qRT-PCR and normalized to EGF expression (defined as 1) (n = 2).

(B) AREG expression by Western blot (n = 2).

(C) Upon serum deprivation for 18 h, cells were stimulated with NE at indicated doses for 10 min. Supernatants were collected and AREG release measured by ELISA. Asterisks indicate differences between NE versus vehicle treatment (n = 3). Data represent mean ± SEM. p values determined by one-way ANOVA Dunnett test. *p < 0.05, **p < 0.01.

(D) Serum-starved cells were pretreated with 5 μg/mL of AREG neutralizing antibody (α-AREG) or goat IgG control antibody for 60 min and then stimulated with NE at indicated doses for 10 min. Cell lysates were immunoblotted with anti-phospho ERK antibody followed by re-probing the same membranes with anti-total ERK and Vinculin antibodies. AREG neutralizing antibody regulated pERK inhibitions quantified and displayed on histograms. Asterisks indicate differences between α-AREG + NE versus IgG + NE (n = 3). Data represent mean ± SEM. p values determined by one-way ANOVA Sidak test. ns, not significant. *p < 0.05, **p < 0.01.

See also Figure S3.

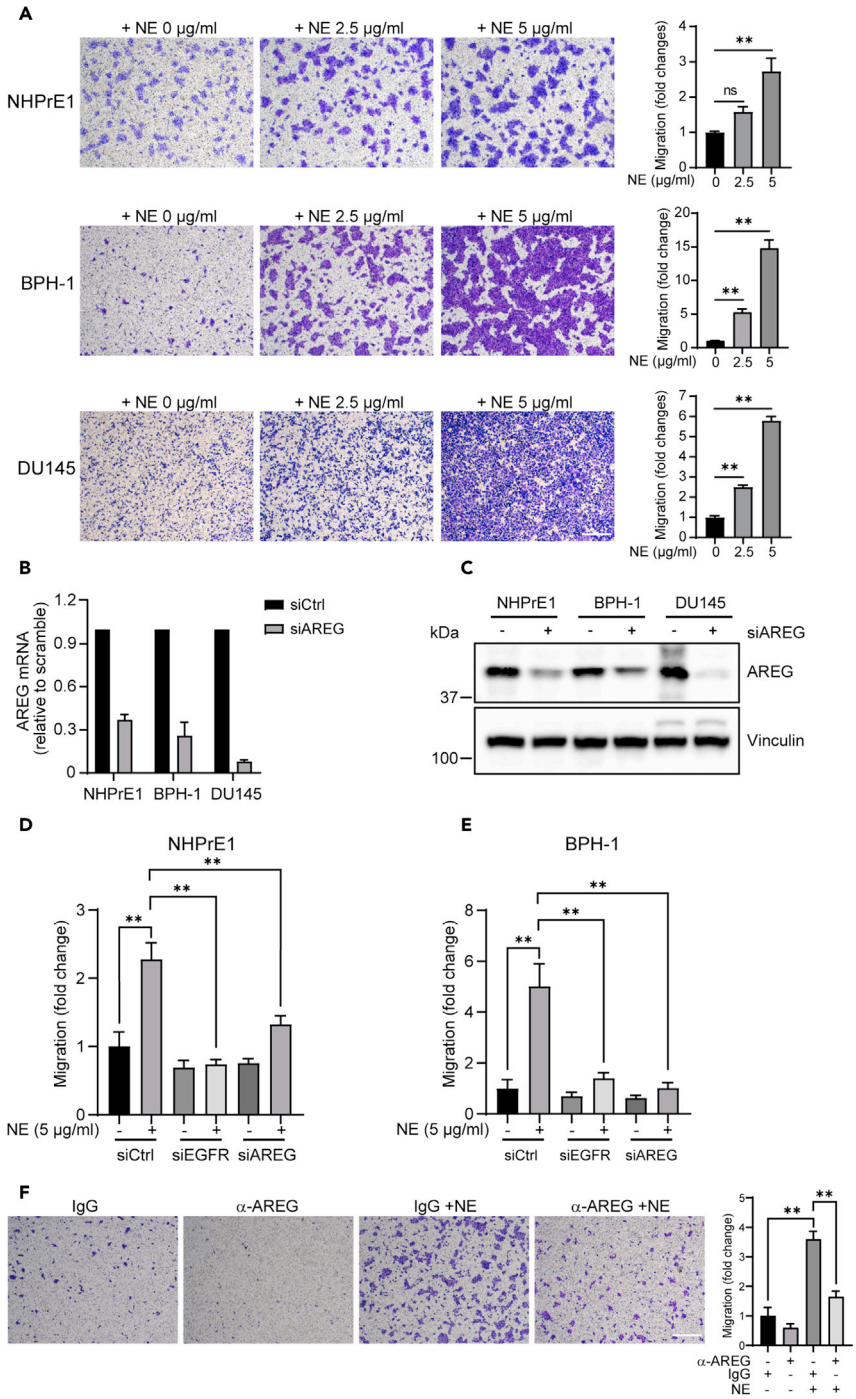

Figure 4. siRNA-mediated knockdown of EGFR or AREG inhibits NE-induced migration of non-malignant prostatic cells

(A) Cells were serum-starved overnight and then analyzed for NE-induced transwell migration. NHPrE1, BPH-1, and DU145 cells were seeded in the upper chamber at a density of $5x10^4$, $1x10^5$, and $5x10^4$ cells/insert, respectively. Representative images shown for cells treated with vehicle (0), 2.5, and 5 µg/mL of NE. The migration ability of each cell line treated with vehicle control was arbitrarily set to 1. Data were normalized to controls. Data represent mean ± SEM from n = 3 experiments. **p < 0.01 by one-way ANOVA Tukey test. ns, not significant. Scale bar: 400 µm.

(B and C) Cells were transfected with siAREG or scramble control (siCtrl) for 72 h and analyzed for AREG expression by qRT-PCR (B) and Western blot (C). Data represent mean ± SEM from n = 3 experiments.

Figure 4. *Continued*

(D and E) siAREG/siEGFR transfected cells were cultured for approximately 50 h and then analyzed for NE-mediated cell migration. NHPrE1 (D) and BPH-1 (E) cells were plated in the upper chamber at a density of $5x10^4$ and $1x10^5$ cells/well, respectively. Cell migration was quantified and displayed on histograms ($n \geq 3$). Data represent mean ± SEM. $^{**}p < 0.01$ by one-way ANOVA Tukey test.

(F) BPH-1 cells, after overnight serum starvation, were trypsinized and pre-incubated with 10 μg/mL of AREG neutralizing antibody (α-AREG) or IgG control antibody for 60 min at 4°C. $5x10^4$ cells mixed with 5 μg/mL of NE were then loaded into the upper chamber for transwell migration assay. Cell migration quantified and displayed on histograms ($n = 3$). Data represent mean ± SEM. $^{**}p < 0.01$ by one-way ANOVA Tukey test. Scale bar: 400 μm.

See also Figure S4.

et al., 2017). Here we extended our work to determine the migration capacity of prostate normal and neoplastic cells in the presence and absence of NE. When treated with 2.5 μg/mL of NE, significantly enhanced migration was seen in neoplastic BPH-1 and DU145 cells, but not normal NHPrE1 cells. Migration was even more pronounced when 5 μg/mL of NE was added in all three cell lines (Figure 4A). NE-induced dose-dependent migration was further seen in PC3 cancer cells (Figure S4A). Notably, migration assays were performed at 24 h; thus, it is possible that the enhanced migration was due in part to NE-mediated changes in proliferation. However, NE induced minimal to no proliferation in BPH-1 and DU145 cells over the same time course (Figure S4B), indicating that proliferation plays a minor role at best in NE-induced migration. In contrast, with NHPrE1 cells (Figure S4B), NE-induced proliferation was modest but slightly more robust, suggesting that, in these "benign" cells, we cannot rule out enhanced proliferation as a component of the observed NE-mediated migratory effects.

Because NE triggers a universal ERK activation in all cell lines tested, we questioned whether blocking ERK phosphorylation using a pharmacological inhibitor of MEK (PD325901) could abrogate cell migration. PD325901-mediated pERK inhibition was confirmed by Western blot (Figure S4C), whereas the inhibition of pERK did not prevent NE-induced migration in DU145 cells (Figure S4D). These results are consistent with studies in C4-2 cells, where MEK inhibition similarly had no effect on NE-mediated migration (Lerman et al., 2017).

Next, we assessed the functional impact of AREG inhibition on NE-induced prostate cell migration. Using AREG siRNAs, we specifically silenced endogenous AREG expression and efficient knockdown of AREG was confirmed by quantitative RT-PCR (Figure 4B) and Western blot (Figure 4C). siAREG caused over 50% protein knockdown in NHPrE1 and BPH-1 cells and over 90% in DU145 cells. EGFR inhibition was performed by using the aforementioned siRNA directed against EGFR. Notably, NE-induced migration was significantly abrogated by EGFR and AREG knockdown in non-malignant NHPrE1 and BPH-1 cells (Figures 4D and 4E).

To evaluate whether enhanced migration is mediated by soluble AREG, we pre-incubated BPH-1 cells with α-AREG prior to NE stimulation. The AREG blockade significantly attenuated NE-induced migration of BPH-1 cells (Figure 4F). These data confirm the importance of NE-mediated AREG release and EGFR activation in regulating migration in non-malignant prostate cells.

In contrast, AREG inhibition with either α-AREG or siRNA (Figures S5A and S5B) had little or no effect on NE-mediated migration in DU145 cancer cells. Furthermore, despite its role in NE-induced ERK activation, EGFR did not appear to be required for NE-mediated migration in these cells, as siRNA-mediated EGFR knockdown did not attenuate NE-induced migration (Figure 5C).

AXL is involved in NE-mediated prostate cancer cell migration

Activation of RTK AXL was previously proposed as a prominent mechanism of acquired resistance to EGFR targeted therapy (Zhang et al., 2012). AXL is aberrantly expressed in various cancers and can modulate cell growth and invasiveness (Gay et al., 2017). With this in mind, we analyzed our panel of prostatic normal and cancer cell lines and detected AXL expression (Figure 5A) in a similar pattern to that of EGFR expression (Figure 2A). Notably, in prostate cancer cell lines, AXL expression was considerably higher in more aggressive DU145 and PC3 cells (Figure 5A).

To establish the relevance of AXL in prostate cancer cell mitogenic signal and migration, we abrogated its expression in DU145 cells using pooled siRNA. In cells transfected with siRNA directed against either EGFR or AXL mRNA, basal levels of pERK were slightly lower than the control cells (Figure 5B). Furthermore, NE

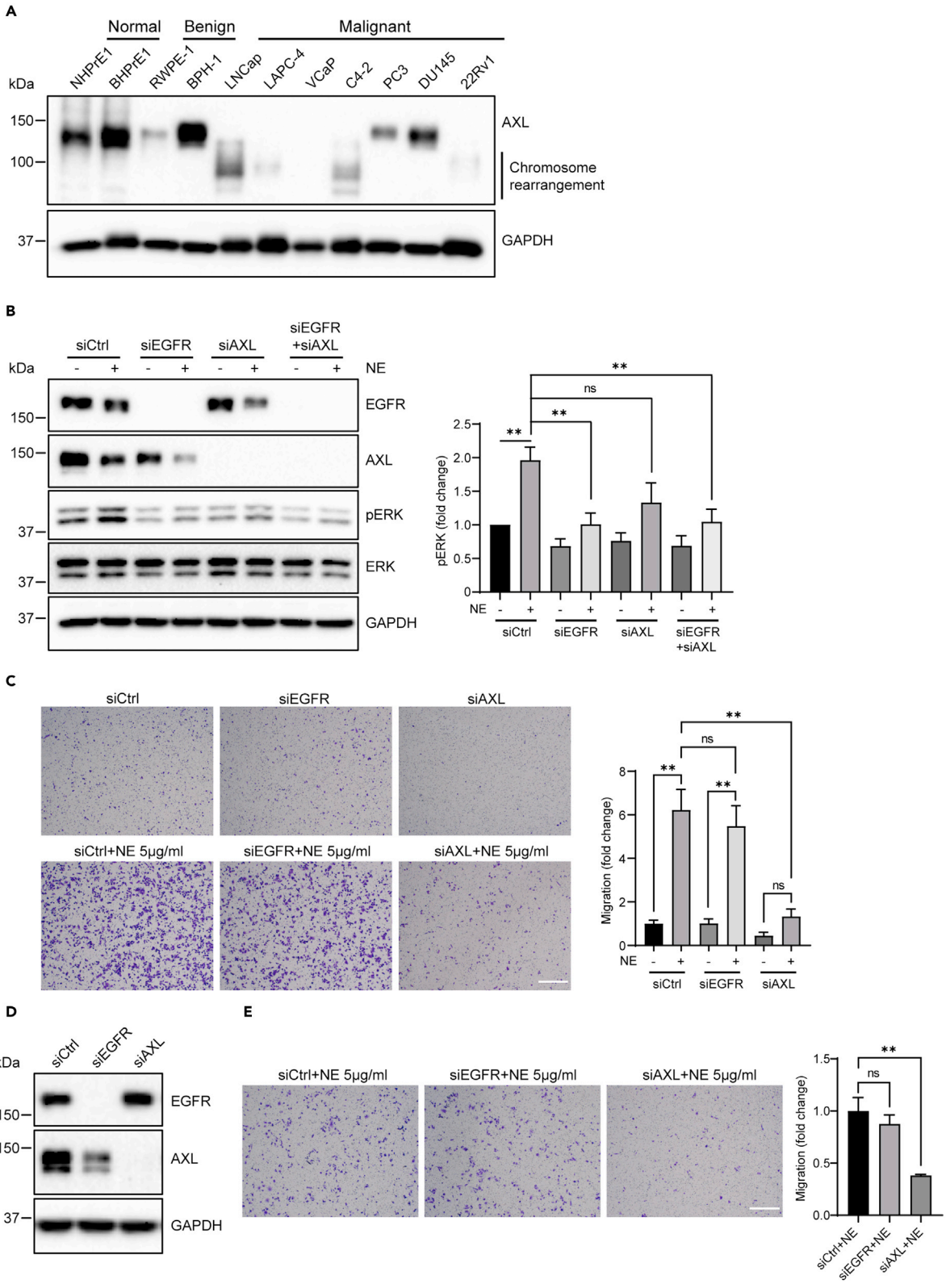
A
Normal
Benign
Malignant
NHPrE1
BHPrE1
RWPE-1
BPH-1
LNCap
LAPC-4
VCaP
C4-2
PC3
DU145
22Rv1
kDa
150
100
37
AXL
Chromosome rearrangement
GAPDH
B
siCtrl
siEGFR
siAXL
siEGFR +siAXL
NE
EGFR
AXL
pERK
ERK
GAPDH
pERK (fold change)
**
ns
C
siCtrl
siEGFR
siAXL
siCtrl+NE 5μg/ml
siEGFR+NE 5μg/ml
siAXL+NE 5μg/ml
Migration (fold change)
D
E

Figure 5. Knockdown of AXL but not EGFR attenuates NE-mediated prostate cancer cell migration

(A) Differential AXL expression by Western blot (n = 2).

(B) DU145 cells transfected for approximately 55 h with EGFR or AXL specific siRNA (siEGFR or siAXL) or scramble control, and then serum-starved overnight prior to 10 min stimulation with NE (0.5 μg/mL) or vehicle. Immunoblots for EGFR, AXL, pERK, ERK, and GAPDH are shown. siEGFR/siAXL mediated pERK inhibitions are quantified and displayed on histograms. Data represent mean ± SEM from n = 4 experiments. **$p < 0.01$ by one-way ANOVA Tukey test. ns, not significant.

(D) siRNA-mediated reduction of EGFR and AXL expression in PC3 cells with 72 h transfection.

(C and E) siEGFR/siAXL transfected cells cultured for approximately 50 h and then analyzed for NE mediated cell migration. DU145 (C) and PC3 (E) cells plated in the upper chamber at a density of $4x10^4$ and $2x10^5$ cells/well, respectively. Cell migration quantified and displayed on histograms. Data represent means ± SEM from $n \geq 3$ experiments. **$p < 0.01$ by one-way ANOVA Tukey test. ns, not significant. Scale bar: 400 μm.

See also Figure S5.

was unable to cause major increases in pERK levels when either receptor tyrosine kinase was reduced in expression, confirming the importance of both EGFR and AXL for NE-induced ERK signaling. In contrast, silencing of EGFR had minimal effect on NE-induced migration, whereas knockdown of endogenous AXL markedly attenuated basal and NE-stimulated migration (Figure 5C). Notably, combination knockdown of both EGFR and AXL did not further suppress the NE-mediated migratory effect relative to AXL knockdown alone (data not shown), suggesting that AXL is acting independently of EGFR to regulate NE-mediated migration in these cells. Similarly, AXL knockdown in PC3 cells resulted in almost complete attenuation of migration in the presence of NE (Figures 5D and 5E). Together, these results indicate that, while both EGFR and AXL are required for NE-induced ERK activation in the prostate cancer cell lines tested, NE-mediated migration requires AXL over EGFR.

DISCUSSION

Myeloid cell-derived NE is known to play an important role in the progression of many different cancers (Houghton et al., 2010; Deryugina et al., 2020; Caruso et al., 2015), including prostate (Lerman et al., 2017). This study provides new insights into the molecular events regulating NE-induced mitogenic signaling and migration in preneoplastic prostate and cancer cells by activating dual EGFR and AXL signaling cascades.

By immunofluorescence and Western blot analysis, we demonstrate rapid dynamin-mediated intracellular trafficking of NE in prostate cells that lack endogenous NE expression. These observations are consistent with other studies showing NE endocytosis in cancer cells, including lung, ovarian, colon, and breast (Houghton et al., 2010; Alatrash et al., 2012; Gregory et al., 2012; Mittendorf et al., 2012; Kerros et al., 2017). However, in our study, NE uptake varied considerably depending on the potential malignancy of the cell lines, ranging from the least in NHPrE1 normal prostate epithelium cells to the highest in aggressive DU145 carcinoma cells. We propose that the stem-like properties of NHPrE1 cells may contribute to efficient NE efflux, preventing significant intracellular accumulation. NE import has been associated with intracellular cleavage of IRS1 and subsequent activation of the PI3K/AKT pathway in lung adenocarcinoma cells (Houghton et al., 2010; Gregory et al., 2012). However, regardless of the accessibility of NE in prostate cell lines tested, analysis of NE-induced AKT signaling did not reveal significant activation of this pathway (data not shown). Instead, we saw compelling NE-mediated activation of ERK signaling, which occurred even when NE uptake was effectively inhibited. Thus, the consequence of NE internalization in prostate cells remains unclear.

Our data strongly implicate extracellular functions of NE in promoting ERK signaling via activation of RTKs such as EGFR. This is in agreement with the previous work showing that in lung fibroblasts and cancer cells, NE initiates EGFR/MEK/ERK signaling (DiCamillo et al., 2002, 2006; Song et al., 2005). In addition to androgens, recent advances suggest that the EGFR ligands, through autocrine or paracrine networks, may play important roles during the process of prostate cancer development. For instance, the prostate gland secretes large amounts of EGF (Marti et al., 1989). Accordingly, monolayer culture of preneoplastic prostate cells, including NHPrE1 and BHPrE1 used in our study, requires EGF, not androgen, as a supplement for cell growth. In contrast, TGFA is found primarily in stromal cells at early-stage cancer. Loss of cell contact inhibition elevates TGFA secretion in advanced androgen-independent tumor cells (DeHaan et al., 2009). EGF and TGFA, to our knowledge, are the only EGFR ligands currently described to promote EGFR/ERK signaling and cell migration in response to NE (DiCamillo et al., 2002; Kohri et al., 2002; Wada et al., 2006).

Here we found AREG, of seven EGFR agonists, the most abundant transcript expressed in all tested prostate cell lines representing different stages of tumor progression. AREG protein further exhibited higher expression in normal and benign prostate cell lines relative to the prostate cancer cell lines, suggesting that AREG might play a more important role in preneoplastic prostate growth versus carcinogenesis. Furthermore, ELISA analysis demonstrated that NE releases AREG to activate EGFR-dependent downstream mitogenic signaling. These data are supported by the finding that functional blocking of soluble AREG significantly inhibited NE-triggered ERK activation. In NHPrE1 and DU145 cells, the partial reduction of pERK following the addition of anti-AREG neutralizing antibodies, suggests other mechanisms of autonomous cell growth regulation are potentially active. The molecular mechanism of how NE triggers the release of AREG is not explored in our study. It is possible that NE employs its protease function by directly cleaving membrane-bound AREG, or more likely by first activating other sheddases. Several ADAM family members have been shown to mediate EGFR transactivation induced by G protein-coupled receptor agonists in various cell types. For example, in squamous cell carcinoma SCC-9 cells, ADAM17 mediates AREG shedding and EGFR transactivation by LPA (Gschwind et al., 2003). Other studies also showed NE, by activating ADAM17, induces TGFA release and mucin production in airway epithelial cells (Shao and Nadel, 2005; Kohri et al., 2002).

Despite the great homology with EGF (38%) and TGFA (32%) (Busser et al., 2011), AREG has a significantly lower affinity for EGFR, which makes it less effective in inducing EGFR tyrosine phosphorylation (Macdonald-Obermann and Pike, 2014). Likewise, NE-initiated EGFR phosphorylation in our tested prostate cells is minimal. It is documented that AREG exhibits an exclusive activation of EGFR (Shin et al., 2003). For further confirmation, it will be important to examine the effect of NE on the activation of other ErbB members (HER2, HER3, and HER4) in prostate cell settings.

Aberrant EGFR expression was frequently detected in prostate cancer tissues associated with high-grade advanced stages (Schlomm et al., 2007; Hashmi et al., 2019), suggesting EGFR may play a mechanistic role in the progression of prostate cancer. Therefore, EGFR-targeted therapy can be a potential treatment option. Unfortunately, despite the promising results brought by preclinical studies, EGFR tyrosine kinase inhibitor Gefitinib in clinical trials has shown little activity as a monotherapy or in combination with Docetaxel, a standard first-line treatment for hormone-refractory prostate cancer (Canil et al., 2005; Gross et al., 2007). In accordance with the clinical studies, silencing of EGFR and AREG had little or no effect on NE-mediated migration in prostate cancer cells. Instead, AXL was highly expressed in advanced DU145 and PC3 prostatic cancer cells, and knockdown of AXL almost completely abrogated NE-induced migration in both cell lines. The switch from an EGFR-to AXL-dependent mechanism in cell migration stresses the role of AXL in prostate cancer progression. Notably, clinical trials are already underway using AXL inhibition to treat several different types of cancer (Zhu et al., 2019). Therefore, the potential utility of anti-AXL treatments could be analyzed in EGFR-expressing prostate cancer.

AXL, a member of the TAM (TYRO3, AXL, and MER) family of RTK, is overexpressed in several hematologic and solid tumors, including the prostate. Evidence suggests that aberrant AXL expression regulates diverse cellular processes, including epithelial to mesenchymal transition, angiogenesis, and decreased antitumor immune response and therapeutic resistance (Gay et al., 2017; Vajkoczy et al., 2006). Consistent with our findings, in prostate cancer cell lines, AXL signaling is important in regulating mitogenic activity (Sainaghi et al., 2005), with AXL knockdown leading to decreased cell proliferation, migration, invasion, and tumor growth (Mishra et al., 2012; Shiozawa et al., 2010; Paccez et al., 2013). Canonical activation of AXL signaling requires its specific ligand-growth arrest-specific protein 6 (GAS6) (Sasaki et al., 2006). NE may regulate the release of soluble GAS6, which then activates AXL for diverse cellular responses. However, we could not detect GAS6 in the media of NE-treated DU145 cells, nor did GAS6 neutralizing antibodies interfere with NE-induced cell migration (data not shown). Therefore, we propose a GAS6-independent mechanism of AXL activation, e.g., overexpression induced homotypic aggregation of AXL extracellular domains on adjacent cells (Bellosta et al., 1995) or heterodimerization with other transmembrane receptors such as EGFR, MET (hepatocyte growth factor receptor), PDGF (platelet-derived growth factor), and VEGFR-2 (vascular endothelial growth factor receptor-2) (Meyer et al., 2013; Ruan and Kazlauskas, 2012), to initiate downstream programs in prostate cancer cells.

In summary, our study demonstrates an essential role of the AREG-EGFR signaling axis in NE-triggered prostatic cellular responses. AXL may act as a cooperative player in more advanced prostate cancer,

both in response to NE from the innate immune response as well as to other external signaling that might drive prostate cancer progression. Given our data, a combination of EGFR and AXL targeted therapy may serve as a potential therapeutic option in advanced prostate cancer treatment.

Limitations of the study

Although our studies reveal that NE promotes EGFR activation and migration in non-malignant prostate cells via amphiregulin release, we have not yet determined precisely how NE triggers amphiregulin ectodomain shedding in those cells. In addition, although we discovered that NE promotes prostate cancer cell migration via AXL rather than EGFR, the mechanisms behind this NE-mediated AXL activation remain undetermined. Finally, although our results are robust and consistent in multiple prostate cell lines, future studies will need to focus on *in vivo* application of EGFR and AXL targeted therapy in prostate cancer treatment.

STAR★METHODS

Detailed methods are provided in the online version of this paper and include the following:

- KEY RESOURCES TABLE
- RESOURCE AVAILABILITY
  - Lead contact
  - Materials availability
  - Data and code availability
- EXPERIMENTAL MODEL AND SUBJECT DETAILS
  - Human prostate cell lines
- METHOD DETAILS
  - Cell signaling studies with human neutrophil elastase
  - Cell proliferation assay
  - Enzyme-linked immunosorbent assay (ELISA)
  - Western blot analysis
  - Quantitative RT-PCR (qRT-PCR)
  - Immunofluorescence staining
  - Small interfering RNA (siRNA) transfection
  - Boyden chamber migration assay
- QUANTIFICATION AND STATISTICAL ANALYSIS
  - Statistical analysis

SUPPLEMENTAL INFORMATION

Supplemental information can be found online at https://doi.org/10.1016/j.isci.2021.103270.

ACKNOWLEDGMENTS

We thank Dr. Pjotr Kynazev for helpful discussion on the project. NHPrE1 and BHPrE1 cell lines were gifts from Dr. Simon W. Hayward (NorthShore University HealthSystem). This study is supported by National Institutes of Health grant R01 CA193583.

AUTHOR CONTRIBUTIONS

Z.X. and S.R.H. designed the work and wrote the paper. Z.X. conducted the experiments.

DECLARATION OF INTERESTS

The authors declare no competing interests.

Received: May 2, 2021
Revised: June 28, 2021
Accepted: October 12, 2021
Published: November 19, 2021

REFERENCES

Alatrash, G., Mittendorf, E.A., Sergeeva, A., Sukhumalchandra, P., Qiao, N., Zhang, M., John, L.S.S., Ruisaard, K., Haugen, C.E., and Al-Atrache, Z. (2012). Broad cross-presentation of the hematopoietically derived PR1 antigen on solid tumors leads to susceptibility to PR1-targeted immunotherapy. J. Immunol. *189*, 5476–5484.

Bellosta, P., Costa, M., Lin, D.A., and Basilico, C. (1995). The receptor tyrosine kinase ARK mediates cell aggregation by homophilic binding. Mol. Cell Biol. *15*, 614–625.

Busser, B., Sancey, L., Brambilla, E., Coll, J.-L., and Hurbin, A. (2011). The multiple roles of amphiregulin in human cancer. Biochim. Biophys. Acta Rev. Canc. *1816*, 119–131.

Canil, C., Moore, M., Winquist, E., Baetz, T., Pollak, M., Chi, K., Berry, S., Ernst, D., Douglas, L., and Brundage, M. (2005). Randomized phase II study of two doses of gefitinib in hormone-refractory prostate cancer: a trial of the National Cancer Institute of Canada-Clinical Trials Group. J. Clin. Oncol. *23*, 455–460.

Caruso, J.A., Akli, S., Pageon, L., Hunt, K.K., and Keyomarsi, K. (2015). The serine protease inhibitor elafin maintains normal growth control by opposing the mitogenic effects of neutrophil elastase. Oncogene *34*, 3556–3567.

De Muga, S., Hernández, S., Agell, L., Salido, M., Juanpere, N., Lorenzo, M., Lorente, J.A., Serrano, S., and Lloreta, J. (2010). Molecular alterations of EGFR and PTEN in prostate cancer: association with high-grade and advanced-stage carcinomas. Mod. Pathol. *23*, 703–712.

DeHaan, A.M., Wolters, N.M., Keller, E.T., and Ignatoski, K.M.W. (2009). EGFR ligand switch in late stage prostate cancer contributes to changes in cell signaling and bone remodeling. Prostate *69*, 528–537.

Deryugina, E., Carré, A., Ardi, V., Muramatsu, T., Schmidt, J., Pham, C., and Quigley, J.P. (2020). Neutrophil elastase facilitates tumor cell intravasation and early metastatic events. Iscience *23*, 101799.

Di Lorenzo, G., Tortora, G., D'Armiento, F.P., De Rosa, G., Staibano, S., Autorino, R., D'Armiento, M., De Laurentiis, M., De Placido, S., and Catalano, G. (2002). Expression of epidermal growth factor receptor correlates with disease relapse and progression to androgen-independence in human prostate cancer. Clin. Cancer Res. *8*, 3438–3444.

DiCamillo, S.J., Carreras, I., Panchenko, M.V., Stone, P.J., Nugent, M.A., Foster, J.A., and Panchenko, M.P. (2002). Elastase-released epidermal growth factor recruits epidermal growth factor receptor and extracellular signal-regulated kinases to down-regulate tropoelastin mRNA in lung fibroblasts. J. Biol. Chem. *277*, 18938–18946.

DiCamillo, S.J., Yang, S., Panchenko, M.V., Toselli, P.A., Naggar, E.F., Rich, C.B., Stone, P.J., Nugent, M.A., and Panchenko, M.P. (2006). Neutrophil elastase-initiated EGFR/MEK/ERK signaling counteracts stabilizing effect of autocrine TGF-beta on tropoelastin mRNA in lung fibroblasts. Am. J. Physiol. Lung Cell Mol. Physiol. *291*, L232–L243.

Foekens, J.A., Ries, C., Look, M.P., Gippner-Steppert, C., Klijn, J.G., and Jochum, M. (2003). The prognostic value of polymorphonuclear leukocyte elastase in patients with primary breast cancer. Cancer Res. *63*, 337–341.

Gay, C.M., Balaji, K., and Byers, L.A. (2017). Giving AXL the axe: targeting AXL in human malignancy. Br. J. Cancer *116*, 415–423.

Gregory, A.D., Hale, P., Perlmutter, D.H., and Houghton, A.M. (2012). Clathrin pit-mediated endocytosis of neutrophil elastase and cathepsin G by cancer cells. J. Biol. Chem. *287*, 35341–35350.

Gross, M., Higano, C., Pantuck, A., Castellanos, O., Green, E., Nguyen, K., and Agus, D.B. (2007). A phase II trial of docetaxel and erlotinib as first-line therapy for elderly patients with androgen-independent prostate cancer. BMC Cancer *7*, 142.

Gschwind, A., Hart, S., Fischer, O.M., and Ullrich, A. (2003). TACE cleavage of proamphiregulin regulates GPCR-induced proliferation and motility of cancer cells. EMBO J. *22*, 2411–2421.

Gusenbauer, S., Zanucco, E., Knyazev, P., and Ullrich, A. (2015). Erk2 but not Erk1 regulates crosstalk between Met and EGFR in squamous cell carcinoma cell lines. Mol. Cancer *14*, 1–7.

Hashmi, S.K., Irfan, M., Asif, H., Nisar, L., Naeem, M., Khan, E.Y., Baloch, S., and Faridi, N. (2019). Prognostic utility of epidermal growth factor receptor (EGFR) expression in prostatic acinar adenocarcinoma. Appl. Cancer Res. *39*, 2.

Ho, A.-S., Chen, C.-H., Cheng, C.-C., Wang, C.-C., Lin, H.-C., Luo, T.-Y., Lien, G.-S., and Chang, J. (2014). Neutrophil elastase as a diagnostic marker and therapeutic target in colorectal cancers. Oncotarget *5*, 473.

Houghton, A.M., Rzymkiewicz, D.M., Ji, H., Gregory, A.D., Egea, E.E., Metz, H.E., Stolz, D.B., Land, S.R., Marconcini, L.A., Kliment, C.R., et al. (2010). Neutrophil elastase-mediated degradation of IRS-1 accelerates lung tumor growth. Nat. Med. *16*, 219–223.

Iwatsuki, K.-C., Kumara, E., Yoshimine, T.-C., Nakagawa, H.-C., Sato, M., and Hayakawa, T. (2000). Elastase expression by infiltrating neutrophils in gliomas. Neurol. Res. *22*, 465–468.

Kambhampati, S., Ray, G., Sengupta, K., Reddy, V.P., Banerjee, S.K., and Van Veldhuizen, P.J. (2005). Growth factors involved in prostate carcinogenesis. Front. Biosci. *10*, 1355–1367.

Kerros, C., Tripathi, S.C., Zha, D., Mehrens, J.M., Sergeeva, A., Philips, A.V., Qiao, N., Peters, H.L., Katayama, H., and Sukhumalchandra, P. (2017). Neuropilin-1 mediates neutrophil elastase uptake and cross-presentation in breast cancer cells. J. Biol. Chem. *292*, 10295–10305.

Kohri, K., Ueki, I.F., and Nadel, J.A. (2002). Neutrophil elastase induces mucin production by ligand-dependent epidermal growth factor receptor activation. Am. J. Physiol. Lung Cell Mol. Physiol. *283*, L531–L540.

Korkmaz, B., Horwitz, M.S., Jenne, D.E., and Gauthier, F. (2010). Neutrophil elastase, proteinase 3, and cathepsin G as therapeutic targets in human diseases. Pharmacol. Rev. *62*, 726–759.

Kuwahara, I., Lillehoj, E.P., Lu, W., Singh, I.S., Isohama, Y., Miyata, T., and Kim, K.C. (2006). Neutrophil elastase induces IL-8 gene transcription and protein release through p38/NF-κB activation via EGFR transactivation in a lung epithelial cell line. Am. J. Physiol. Lung Cell Mol. Physiol. *291*, L407–L416.

Lerman, I., De La Luz Garcia-Hernandez, M., Rangel-Moreno, J., Chiriboga, L., Pan, C., Nastiuk, K.L., Krolewski, J.J., Sen, A., and Hammes, S.R. (2017). Infiltrating myeloid cells exert protumorigenic actions via neutrophil elastase. Mol. Cancer Res. *15*, 1138–1152.

Lerman, I., MA, X., Seger, C., Maolake, A., De La Luz Garcia-Hernandez, M., Rangel-Moreno, J., Ackerman, J., Nastiuk, K.L., Susiarjo, M., and Hammes, S.R. (2019). Epigenetic suppression of SERPINB1 promotes inflammation-mediated prostate cancer progression. Mol. Cancer Res. *17*, 845–859.

Macdonald-Obermann, J.L., and Pike, L.J. (2014). Different epidermal growth factor (EGF) receptor ligands show distinct kinetics and biased or partial agonism for homodimer and heterodimer formation. J. Biol. Chem. *289*, 26178–26188.

Marti, U., Burwen, S.J., and Jones, A.L. (1989). Biological effects of epidermal growth factor, with emphasis on the gastrointestinal tract and liver: an update. Hepatology *9*, 126–138.

Meyer, A.S., Miller, M.A., Gertler, F.B., and Lauffenburger, D.A. (2013). The receptor AXL diversifies EGFR signaling and limits the response to EGFR-targeted inhibitors in triple-negative breast cancer cells. Sci. Signal. *6*, ra66.

Meyer-Hoffert, U. (2009). Neutrophil-derived serine proteases modulate innate immune responses. Front. Biosci. *14*, 3409–3418.

Mishra, A., Wang, J., Shiozawa, Y., Mcgee, S., Kim, J., Jung, Y., Joseph, J., Berry, J.E., Havens, A., and Pienta, K.J. (2012). Hypoxia stabilizes GAS6/Axl signaling in metastatic prostate cancer. Mol. Cancer Res. *10*, 703–712.

Mittendorf, E.A., Alatrash, G., Qiao, N., WU, Y., Sukhumalchandra, P., John, L.S.S., Philips, A.V., Xiao, H., Zhang, M., and Ruisaard, K. (2012). Breast cancer cell uptake of the inflammatory mediator neutrophil elastase triggers an anticancer adaptive immune response. Cancer Res. *72*, 3153–3162.

Paccez, J.D., Vasques, G.J., Correa, R.G., Vasconcellos, J.F., Duncan, K., Gu, X., Bhasin, M., Libermann, T.A., and Zerbini, L.F. (2013). The receptor tyrosine kinase Axl is an essential regulator of prostate cancer proliferation and tumor growth and represents a new therapeutic target. Oncogene *32*, 689.

Pham, C.T. (2006). Neutrophil serine proteases: specific regulators of inflammation. Nat. Rev. Immunol. *6*, 541–550.

Plowman, G., Green, J., McDonald, V., Neubauer, M., Disteche, C., Todaro, G., and Shoyab, M. (1990). The amphiregulin gene encodes a novel

epidermal growth factor-related protein with tumor-inhibitory activity. Mol. Cell Biol. *10*, 1969–1981.

Ruan, G.X., and Kazlauskas, A. (2012). Axl is essential for VEGF-A-dependent activation of PI3K/Akt. EMBO J. *31*, 1692–1703.

Sainaghi, P.P., Castello, L., Bergamasco, L., Galletti, M., Bellosta, P., and Avanzi, G.C. (2005). Gas6 induces proliferation in prostate carcinoma cell lines expressing the Axl receptor. J. Cell. Physiol. *204*, 36–44.

Sasaki, T., Knyazev, P.G., Clout, N.J., Cheburkin, Y., Göhring, W., Ullrich, A., Timpl, R., and Hohenester, E. (2006). Structural basis for Gas6–Axl signalling. EMBO J. *25*, 80–87.

Schlomm, T., Kirstein, P., Iwers, L., Daniel, B., Steuber, T., Walz, J., Chun, F.H., Haese, A., Kollermann, J., and Graefen, M. (2007). Clinical significance of epidermal growth factor receptor protein overexpression and gene copy number gains in prostate cancer. Clin. Cancer Res. *13*, 6579–6584.

Shao, M.X., and Nadel, J.A. (2005). Dual oxidase 1-dependent MUC5AC mucin expression in cultured human airway epithelial cells. Proc. Natl. Acad. Sci. *102*, 767–772.

Shin, H.S., Lee, H.J., Nishida, M., Lee, M.-S., Tamura, R., Yamashita, S., Matsuzawa, Y., Lee, I.-K., and Koh, G.Y. (2003). Betacellulin and amphiregulin induce upregulation of cyclin D1 and DNA synthesis activity through differential signaling pathways in vascular smooth muscle cells. Circ. Res. *93*, 302–310.

Shiozawa, Y., Pedersen, E.A., Patel, L.R., Ziegler, A.M., Havens, A.M., Jung, Y., Wang, J., Zalucha, S., Loberg, R.D., and Pienta, K.J. (2010). GAS6/AXL axis regulates prostate cancer invasion, proliferation, and survival in the bone marrow niche. Neoplasia *12*, 116–IN4.

Siegel, R.L., Miller, K.D., Goding Sauer, A., Fedewa, S.A., Butterly, L.F., Anderson, J.C., Cercek, A., Smith, R.A., and Jemal, A. (2020). Colorectal cancer statistics, 2020. CA Cancer J. Clin. *70*, 145–164.

Song, J.-S., Cho, K.-S., Yoon, H.-K., Moon, H.-S., and Park, S.-H. (2005). Neutrophil elastase causes MUC5AC mucin synthesis via EGF receptor, ERK and NF-kB pathways in A549 cells. Kor. J. Intern. Med. *20*, 275.

Starcher, B., O'Neal, P., Granstein, R.D., and Beissert, S. (1996). Inhibition of neutrophil elastase suppresses the development of skin tumors in hairless mice. J. Invest. Dermatol. *107*, 159–163.

Vajkoczy, P., Knyazev, P., Kunkel, A., Capelle, H.-H., Behrndt, S., Von Tengg-Kobligk, H., Kiessling, F., Eichelsbacher, U., Essig, M., and Read, T.-A. (2006). Dominant-negative inhibition of the Axl receptor tyrosine kinase suppresses brain tumor cell growth and invasion and prolongs survival. Proc. Natl. Acad. Sci. *103*, 5799–5804.

Wada, Y., Yoshida, K., Tsutani, Y., Shigematsu, H., Oeda, M., Sanada, Y., Suzuki, T., Mizuiri, H., Hamai, Y., and Tanabe, K. (2006). Neutrophil elastase induces cell proliferation and migration by the release of TGF-α, PDGF and VEGF in esophageal cell lines. Oncol. Rep. *17*, 161–167.

Yamashita, J.-I., Ogawa, M., Abe, M., Hayashi, N., Kurusu, Y., Kawahara, K., and Shirakusa, T. (1997). Tumor neutrophil elastase is closely associated with the direct extension of non-small cell lung cancer into the aorta. Chest *111*, 885–890.

Zhang, Z., Lee, J.C., Lin, L., Olivas, V., Au, V., Laframboise, T., Abdel-Rahman, M., Wang, X., Levine, A.D., and Rho, J.K. (2012). Activation of the AXL kinase causes resistance to EGFR-targeted therapy in lung cancer. Nat. Genet. *44*, 852–860.

Zhu, C., Wei, Y., and Wei, X. (2019). AXL receptor tyrosine kinase as a promising anti-cancer approach: functions, molecular mechanisms and clinical applications. Mol. Cancer *18*, 153.

STAR★METHODS

KEY RESOURCES TABLE

REAGENT or RESOURCE	SOURCE	IDENTIFIER
Antibodies		
Rabbit Polyclonal anti-Neutrophil elastase	Abcam	Cat# ab68672; RRID:AB_1658868
Mouse monoclonal anti-Neutrophil Elastase (NP57) Alexa Fluor® 488	Santa Cruz Biotechnology	Cat# sc-53388; RRID:AB_630032
Rabbit Polyclonal anti-EGF Receptor	Cell Signaling Technology	Cat# 2232; RRID:AB_331707
Rabbit Polyclonal anti-Phospho-EGF Receptor (Tyr1068)	Cell Signaling Technology	Cat# 2234; RRID:AB_331701
Rabbit Polyclonal anti- p44/42 MAPK (Erk1/2)	Cell Signaling Technology	Cat# 9102; RRID:AB_330744
Rabbit Polyclonal anti- p44/42 MAP kinase (phosphorylated Erk1/2) antibody	Cell Signaling Technology	Cat# 9101; RRID:AB_331646
Rabbit Polyclonal anti-Amphiregulin	Proteintech	Cat# 16036-1-AP; RRID:AB_2227602
Mouse monoclonal anti-GAPDH	Abcam	Cat# ab9484; RRID:AB_307274
Mouse monoclonal anti-Vinculin	Santa Cruz Biotechnology	Cat# sc-73614; RRID:AB_1131294
Goat Polyclonal anti-AXL	R&D Systems	Cat# AF154; RRID:AB_354852
Goat Polyclonal anti-Amphiregulin	R&D Systems	Cat# AF262; RRID:AB_2243124
Goat Polyclonal IgG Control	R&D Systems	Cat# AB-108-C; RRID:AB_354267
Goat Anti-Rabbit IgG (H L)-HRP Conjugate antibody	Bio-Rad	Cat# 170-6515; RRID:AB_11125142
Goat Anti-Mouse IgG (H L)-HRP Conjugate antibody	Bio-Rad	Cat# 170-6516; RRID:AB_11125547
Rabbit Anti-Goat IgG (H L)-HRP Conjugate antibody	Bio-Rad	Cat# 172-1034; RRID:AB_11125144
Chemicals, peptides, and recombinant proteins		
Human Neutrophil Elastase	Molecular Innovations	SKU: HNE-L
EGF Recombinant Human Protein	Thermo Fisher Scientific	Cat# PHG0311
N-(3-chlorophenyl)-6,7-dimethoxyquinazolin-4-amine (AG1478)	Sigma-Aldrich	Cat# 658548; CAS: 175178-82-2
N-[(E)-(3,4-dihydroxyphenyl)methylideneamino]-3-hydroxynaphthalene-2-carboxamide;hydrate (Dynasore)	Sigma-Aldrich	Cat# D7693; CAS: 1202867-00-2
N-[(2R)-2,3-dihydroxypropoxy]-3,4-difluoro-2-(2-fluoro-4 iodoanilino)benzamide (PD0325901)	Selleckchem	Cat# S1036; CAS 391210-10-9
Critical commercial assays		
Human Amphiregulin Quantikine ELISA Kit	R&D Systems	Cat# DAR00
RNeasy Plus Mini Kit	QIAGEN	Cat# 74134
BrdU Cell Proliferation Assay Kit	Cell Signaling Technology	Cat# 6813
Deposited data		
Original western blot images	This paper	Mendeley at https://doi.org/10.17632/6x8r2kt6ky.1
Experimental models: Cell lines		
Human prostate NHPrE1	Simon W. Hayward, NorthShore University HealthSystem	N/A
Human prostate BHPrE1	Simon W. Hayward, NorthShore University HealthSystem	N/A
Human prostate RWPE-1	ATCC	RRID:CVCL_3791

(*Continued on next page*)

Continued

REAGENT or RESOURCE	SOURCE	IDENTIFIER
Human prostate BPH-1	Donald DeFranco, University of Pittsburgh	RRID:CVCL_1091
Human prostate LAPC-4	Kent Nastiuk, University at Buffalo	RRID:CVCL_4744
Human prostate Vcap	Kent Nastiuk, University at Buffalo	RRID:CVCL_2235
Human prostate DU145	Kent Nastiuk, University at Buffalo	RRID:CVCL_0105
Human prostate 22Rv1	Kent Nastiuk, University at Buffalo	RRID:CVCL_1045
Human prostate LNCaP	Ganesh Raj, University of Texas Southwestern	RRID:CVCL_0395
Human prostate PC3	Ganesh Raj, University of Texas Southwestern	RRID:CVCL_0035
Human prostate C4-2	Ganesh Raj, University of Texas Southwestern	RRID:CVCL_4782
Oligonucleotides		
Human epidermal growth factor (EGF)	Applied Biosystems	Assay ID: Hs01099990_m1
Human heparin-binding EGF-like growth factor (HBEGF)	Applied Biosystems	Assay ID: Hs00811813_m1
Human transforming growth factor-alpha (TGFA)	Applied Biosystems	Assay ID: Hs00608187_m1
Human epigen (EPGN)	Applied Biosystems	Assay ID: Hs02385424_m1
Human betacellulin (BTC)	Applied Biosystems	Assay ID: Hs01101201_m1
Human amphiregulin (AREG)	Applied Biosystems	Assay ID: Hs00950669_m1
Human epiregulin (EREG)	Applied Biosystems	Assay ID: Hs00914313_m1
Human GAPDH	Applied Biosystems	Assay ID: Hs02786624_g1
EGFR siRNA	Dharmacon	L-003114-00-0005
AREG siRNA	Dharmacon	L-017435-00-0005
AXL siRNA	Dharmacon	L-003104-00-0005
siRNA non-targeting control Pool	Dharmacon	D-001810-10
Software and algorithms		
ImageJ 1.52	NIH	https://imagej.nih.gov/ij/
GraphPad Prism 8.2.0.	GraphPad Prism	https://www.graphpad.com/
Photoshop	Adobe	https://www.adobe.com/products/photoshop.html
Other		
NuPAGE™ LDS Sample Buffer	Invitrogen	Cat# NP0007
qScript XLT one-Step RT-qPCR ToughMix Kit	QuantaBio	Cat# 89236-672
Clarity Western ECL Substrate	Bio-Rad	Cat# 1705061
PVDF membrane	Bio-Rad	Cat# 1620177
RIPA buffer	Thermo Fisher Scientific	Cat# 89900
Halt™ protease and phosphatase inhibitor cocktail	Thermo Fisher Scientific	Cat# 78441
Nunc™ Lab-Tek™ 4-well chamber slides	Thermo Fisher Scientific	Cat# 177399
Lipofectamine™ RNAiMAX	Thermo Fisher Scientific	Cat# 13778075
Insulin-Transferrin-Selenium-Ethanolamine (ITS -X)	Thermo Fisher Scientific	Cat# 51500056
VECTASHIELD® HardSet™ Antifade Mounting Medium with DAPI	Vector Laboratories	Cat# H-1500
Bovine Pituitary Extract	Hammond Cell Tech	Cat# 1078-NZ
Transwell	Corning	Cat# 29442-120

RESOURCE AVAILABILITY

Lead contact

Further information and requests for resources and data should be directed to and will be fulfilled by the lead contact, Zhiguang Xiao (Zhiguang_Xiao@urmc.rochester.edu).

Materials availability

This study did not generate new unique reagents.

Data and code availability

- Original western blot images have been deposited at Mendeley and are publicly available as of the date of publication. The DOI is listed in the key resources table.
- This paper does not report original code.
- Any additional information required to reanalyze the data reported in this paper is available from the lead contact upon request.

EXPERIMENTAL MODEL AND SUBJECT DETAILS

Human prostate cell lines

Human prostate NHPrE1 and BHPrE1 cells (from Simon W. Hayward, NorthShore University HealthSystem, IL) were cultured in DMEM/F12 (Gibco) supplemented with 5% fetal bovine serum (FBS, Seradigm), 1% insulin-transferrin-selenium-Ethanolamine (ITS-X, Gibco), 0.4% bovine pituitary extract (BPE, Hammond Cell Tech), 10 ng/ml EGF (Thermo Scientific), and 1% penicillin-streptomycin (P/S, Gibco). RWPE-1 cells (RRID:CVCL_3791) (American Type Culture Collection (ATCC)) were cultured in keratinocyte serum-free medium (Gibco) supplemented with 25 μg/mL BPE (Gibco), 5 ng/mL EGF (Gibco) and 1% P/S. BPH-1 (RRID:CVCL_1091) (from Donald DeFranco, University of Pittsburgh, PA), LAPC-4 (RRID:CVCL_4744), DU145 (RRID:CVCL_0105), 22Rv1 (RRID:CVCL_1045) (from Kent Nastiuk, University at Buffalo, NY), LNCaP (RRID:CVCL_0395), PC3 (RRID:CVCL_0035) and C4-2 (RRID:CVCL_4782) cells (from Ganesh Raj, University of Texas Southwestern, TX) were cultured in RPMI-1640 (Gibco) supplemented with 10% FBS and 1% P/S. VCaP cells (RRID:CVCL_2235) (from Kent Nastiuk) were cultured in DMEM (Gibco) supplemented with 10% FBS and 1% P/S. All cells were maintained in 5% CO2 at 37°C. For NHPrE1 and BHPrE1 cells, cell morphological changes that indicate differentiation were monitored, and fresh medium was added daily.

METHOD DETAILS

Cell signaling studies with human neutrophil elastase

NHPrE1, BHPrE1, RWPE1, BPH-1, PC3 and DU145 cells were seeded in 6-well plates at 3 x 10^5, 4 x 10^5, 3 x 10^5, 2 x 10^5, 4 x 10^5 and 3 x 10^5 cells/well, respectively. The next day the cells were gently rinsed with PBS to remove all serum, and then starved 18 h in corresponding basal medium (DMEM/F12 for NHPrE1, BHPrE1 cells, keratinocyte serum-free medium for RWPE1 cells, and RPMI-1640 for BPH-1, PC3, and DU145 cells). Human Neutrophil Elastase (NE, Molecular Innovations) at the indicated concentrations were added directly into the starved medium for 10 min. For inhibitory studies, prior to NE stimulation, cells were pretreated with AG1478 (500 nM in DMSO) (#658548, Sigma-Aldrich) or Dynasore (80 μM in DMSO) (#D7693, Sigma-Aldrich) for 30 min, or with amphiregulin-neutralizing antibody (5 μg/mL in PBS) (AF262, R&D Systems) or normal Goat IgG control (5 μg/mL in PBS) (AB-108-C, R&D Systems) for 60 min. NE was prepared at 1 mg/mL stock in 0.05 M Na Acetate pH 5.0 containing 0.1 M NaCl.

Cell proliferation assay

NHPrE1, BPH-1 and DU145 cells were seeded in 96-well plate overnight at 1.5x10^4, 1x10^4 and 1.5x10^4 cells/well, respectively. Cells were then starved in corresponding basal medium overnight. Human NE at the indicated concentrations, along with 10 μM BrdU, were added to the plate and cells were incubated for 24 h. Cell proliferation was assessed using the BrdU Cell Proliferation Assay Kit (#6813, Cell Signaling Technology).

Enzyme-linked immunosorbent assay (ELISA)

As above, cells were serum-starved for 18 h prior to 10 min of NE stimulation. Supernatants were collected, centrifuged at 2000 rpm for 10 min at 4°C to remove cellular debris, and frozen at -80°C in aliquots. Amphiregulin protein was measured using sandwich ELISA (DAR00, R&D Systems). The absorbance at 450 nm was read with a reference wavelength of 540 nm using an ELISA plate reader.

Western blot analysis

Cells were washed once with cold PBS and lysed in RIPA buffer (#89900, Thermo Fisher Scientific) supplemented with 1× Halt™ protease and phosphatase inhibitor cocktail (Thermo Fisher Scientific). Insoluble

cell fragments were removed under centrifugation at 13,000 × g for 20 min at 4°C. Protein lysates along with NuPAGE™ LDS Sample Buffer (NP0007, Invitrogen) were heated at 70°C for 10 min, separated on 7.5, 10, or 12.5% SDS–PAGE, and transferred to PVDF membranes (#1620177, Bio-Rad). The primary antibodies were used against pEGFR (#2234, Cell Signaling Technology), EGFR (#2232, Cell Signaling Technology), AXL (AF154, R&D), amphiregulin (16036-1-AP, Proteintech), pERK (#9101, Cell Signaling Technology), and ERK (#9102, Cell Signaling Technology), Neutrophil Elastase (ab68672, Abcam), GAPDH (ab9484, Abcam), and Vinculin (#73614, Santa Cruz Biotechnology). Secondary HRP-conjugated anti-rabbit, mouse, and goat (Bio-Rad) antibodies were used and detection was done using Clarity Western ECL Substrate (#1705061, Bio-Rad).

Quantitative RT-PCR (qRT-PCR)

RNA was extracted using the RNeasy Plus Mini Kit (#74134, QIAGEN). All quantitative PCR reactions were carried out in the StepOne plus Real-Time PCR system (Applied Biosystems) using the qScript XLT one-Step RT-qPCR ToughMix Kit (#89236-672, QuantaBio) and TaqMan primers (Applied Biosystems) for the following: human epidermal growth factor (EGF) (Hs01099990_m1), heparin-binding EGF-like growth factor (HBEGF) (Hs00811813_m1), transforming growth factor-alpha (TGFA) (Hs00608187_m1), epigen (EPGN) (Hs02385424_m1), betacellulin (BTC) (Hs01101201_m1), amphiregulin (AREG) (Hs00950669_m1), and epiregulin (EREG) (Hs00914313_m1). Each sample was normalized to GAPDH (Hs02786624_g1) as an internal control. Differential expression was calculated according to the ΔΔCT relative quantification method.

Immunofluorescence staining

NHPrE1, BPH-1, and DU145 cells (7.5 x 10^4 cells) were plated onto Nunc™ Lab-Tek™ 4-well chamber slides (#177399, Thermo Fisher Scientific) and allowed to adhere for 24 h. Cells were then serum-starved overnight. 10 min after stimulation with 2.5 μg/mL human NE, cells were immediately fixed with 4% PFA, permeabilized with 0.3% Triton 100 in PBS, blocked with 10% normal goat serum/0.1% Tween 20 in PBS, and incubated with Alexa Fluor 488-conjugated Neutrophil Elastase antibody (1:100, sc-53388 AF488, Santa Cruz Biotechnology). Coverslips were mounted in VECTASHIELD® HardSet™ Antifade Mounting Medium with DAPI (H-1500, Vector Laboratories). Image acquisition was carried out using an Olympus IX71 inverted microscope and the Olympus cellSens software.

Small interfering RNA (siRNA) transfection

NHPrE1, BPH-1, DU145 and PC3 cells were seeded in 6-well plates in antibiotic-free culture medium at a density of 2 x 10^5, 1.5 x 10^5, 2 x 10^5 and 3 x 10^5 cells/well, respectively. The next day the transfection of siRNA SMARTPool (Dharmacon) specific for EGFR (L-003114-00-0005), AREG (L-017435-00-0005), AXL (L-003104-00-0005) as well as corresponding non-targeting control Pool (D-001810-10) were carried out using Lipofectamine™ RNAiMAX (#13778075, Thermo Fisher Scientific) according to the manufacturer's protocol.

Boyden chamber migration assay

Cells were resuspended in 200 μl of serum-free basal medium containing NE at the indicated concentration or vehicle and plated in Corning Boyden chamber inserts (6.5 mm diameter and 8 μm pore size) in 24-transwell dishes at various densities (specified in figure legends). In the bottom chamber, 750 μl of complete culture medium was added. Cells were permitted to migrate for 24 h, then fixed and stained with 0.5% of crystal violet (Sigma). For each experiment, images of 10 fields from 2 insert wells were captured using Olympus IX71 inverted microscope. The value of the migrated cells was calculated and analyzed with the Photoshop CS3 extended measurement feature.

QUANTIFICATION AND STATISTICAL ANALYSIS

Statistical analysis

Band intensities were quantified using ImageJ 1.52 (NIH) software. Data are presented as mean ± SEM from three independent experiments unless stated otherwise. Statistical analyses were performed using GraphPad Prism 8.2.0. Multiple comparisons were evaluated using one-way or 2way ANOVA, and significance defined as $P < 0.05$. P values were shown on the figures as asterisks: *$P < 0.05$; **$P < 0.01$, $p > 0.05$ was considered not significant (ns). The number of replicates used per condition is provided within the corresponding figure legends.